Quantitative Feedback Theory Velocity Control of a Single-rod Pump-controlled Actuator Using a Novel Flow Compensation Circuit

Guangan Ren[1], Gustavo Koury Costa[2] and Nariman Sepehri[1,*]

[1]*Department of Mechanical Engineering, University of Manitoba, Winnipeg, Manitoba, R3T 5V6, Canada*
[2]*Department of Mechanical Engineering, Federal Institute of Science and Technology of the State of Pernambuco, Recife-PE, Brazil*
E-mail: nariman.sepehri@umanitoba.ca
[*]*Corresponding Author*

Received 02 March 2020; Accepted 23 October 2020;
Publication 01 December 2020

Abstract

This paper employs the quantitative feedback theory (QFT) to design a robust fixed-gain linear velocity controller for a newly developed single-rod pump-controlled actuator. The actuator operates in four quadrants, with a load force becoming resistive or assistive alternatively. The controller also satisfies tracking, stability and sensitivity specifications in the presence of a wide range of system parametric uncertainties. Its performance is examined on an instrumented John Deere JD-48 backhoe. The experimental results show that the controller can maintain the actuator velocity within an acceptable response envelope, despite variation in load mass as high as 163 kg and the hydraulic circuit switching between operating quadrants.

Keywords: Pump-controlled actuator, quantitative feedback theory (QFT), robust control, single-rod cylinder, velocity control.

International Journal of Fluid Power, Vol. 21_2, 235–262.
doi: 10.13052/ijfp1439-9776.2124

Introduction

Generally, hydraulic linear actuators can be classified as valve-controlled or pump-controlled. Traditional valve-controlled actuators are characterized by a low-energy efficiency because of the inevitable throttling losses at control valves. On the other hand, in pump-controlled actuators there are no valves controlling the cylinder flow and, therefore, throttling losses from control valves are eliminated.

Pump-controlled linear actuators generally use single-rod (differential) cylinders in order to provide high output forces and reduce the installation space (Quan et al., 2014). Since the flows entering and leaving a differential cylinder are different, a flow compensation circuit has to be designed (Wang et al., 2012). According to the working principle of such systems, there are four possible operation modes, corresponding to four operational quadrants (Costa and Sepehri, 2019). Figure 1 shows the four most relevant hydraulic circuits developed in the literature. With reference to Figure 1(a), the circuit proposed by Hewett (1994) employed a two-position three-way valve to balance the differential flow. However, it has never been experimentally tested. Figure 1(b) shows a circuit using two pilot operated check valves, developed by Rahmfeld and Ivantysynova (2000). The proposed circuit experienced switching between pumping and motoring modes when light loads were moved at high speeds, and was unstable in some conditions (Wang et al., 2012). Caliskan et al. (2015) employed an underlapped valve in the circuit, as shown in Figure 1(c). The obvious downside was that the oscillations could not be removed at certain velocity conditions. Figure 1(d) shows the circuit designed by Wang et al. (2012). It used a three-position, three-way valve as well as two flow-control valves. However, compensation algorithms had to be implemented for an acceptable performance. Recently, Costa and Sepehri (2019) designed a circuit using a three-position, four-way directional valve and a one-directional flow control valve. This circuit produced a stable response in all operation quadrants, and additional algorithms are not needed.

With respect to the control schemes developed for pump-controlled actuators with single-rod cylinders, PID controllers (Daher et al., 2013; Zhang and Chen, 2014), 'skyhook damper' based controllers (Williamson and Ivantysynova 2009), stability controllers (Daher and Ivantysynova, 2015), and modern control techniques based controllers (Daher and Ivantysynova, 2013) have been developed. However, the robustness of all these control schemes has not been assessed. Wei et al. (2009) designed a self-tuning dead-zone compensation fuzzy logic controller for a pump-controlled single-rod

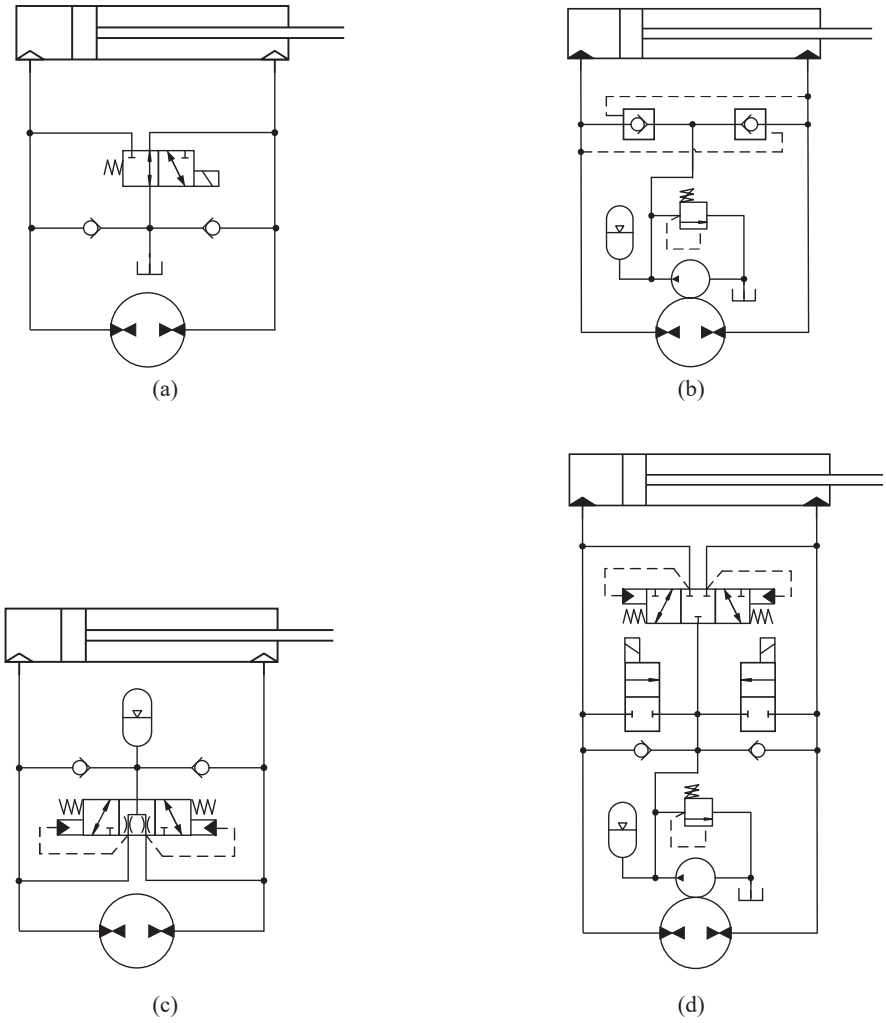

Figure 1 Circuits developed for single-rod pump-controlled actuators designed by (a) Hewett (1994), (b) Rahmfeld and Ivantysynova (2000), (c) Caliskan et al. (2015) and (d) Wang et al. (2012).

hydraulic press. Ahn et al. (2014) proposed a robust position controller using the modified backstepping technique. Daher and Ivantysynova (2014) designed an indirect adaptive velocity controller to adapt to a varying load mass. However, the performance of these controllers was examined in at most two quadrants only.

Quantitative feedback theory (QFT) is an effective way of designing a robust linear controller. It can limit the controller bandwidth by balancing specifications, plant uncertainties, and controller complexity (Yaniv, 1999, Houpis and Rasmussen, 1999). QFT has been successfully applied to design controllers for pump-controlled systems. To name a few, Ren et al. (2016, 2017) proposed QFT controllers that are tolerant to actuator internal leakage. They further designed a low-bandwidth position controller using a system identification technique (Ren et al., 2018). All these controllers are developed for double-rod cylinders. Ahn and Dinh (2009) designed a QFT-based force controller. Truong and Ahn (2009) developed a parallel control strategy using QFT. These force/position controllers were proposed for the circuit developed by Rahmfeld and Ivantysynova (2000) and the actuators worked only in two operating quadrants. Ren et al. (2020) proposed a QFT position controller capable of operating in all quadrants.

This paper presents, for the first time, the design and experimental evaluation of a QFT velocity controller for a single-rod pump-controlled linear actuator, operating in four quadrants. The new circuit described in Costa and Sepehri (2019) is employed. The goal is to design a QFT controller that maintains the actuator velocity within acceptable response envelopes under different loads, and in the presence of system uncertainties. Its performance is examined on a joystick-controlled John Deere JD-48 backhoe, where the displacement of the joystick corresponds to the desired actuator velocity. The novelties of this research are: (i) the design of a robust velocity controller for a single-rod pump-controlled actuator that operates in all four quadrants and (ii), the testing of the controller using a novel circuit applied to a real-world machine.

Modelling and Experimental Setup

Mathematical Model

The schematic drawing of the pump-controlled system investigated in this paper is shown in Figure 2. The system is composed of a bidirectional pump driven by a servomotor, a charge pump connected to a relief valve, a three-position four-way directional valve V1 used to compensate for the unequal flows, a one-directional fixed orifice valve V2 and a single-rod cylinder that acts against a load force, F_L. Check valves, 3 and 4, ensure the actuator chambers do not cavitate while the maximum pressure is set by relief valves 5 and 6. The output pressure of the charge pump is set to 80

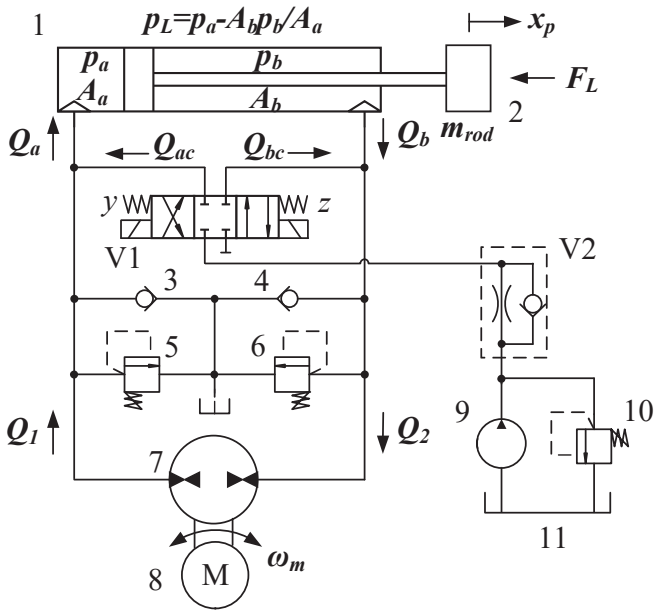

Figure 2 Schematic drawing of the proposed pump-controlled actuator. 1: Actuator. 2: Piston-rod mass. 3: Check valve. 4: Check valve. 5: Relief valve. 6: Relief valve. 7: Bidirectional pump. 8: Servomotor. 9: Charge pump. 10: Relief valve. 11: Tank. V1: Three-position, four-way directional valve. V2: One-directional fixed orifice valve.

psi by the relief valve 10. The working principle of this system is described in Costa and Sepehri (2019). Its four-quadrant working domain is shown in Figure 3. When $p_L > 0$ (Quadrants I and IV), the solenoid y of the directional valve is activated and the solenoid z is deactivated (V1 shifts to left). When $p_L<0$ (Quadrants II and III), the solenoid z is activated, and the solenoid y is deactivated (V1 shifts to right). In order to reduce the effect of noise in the switching of the directional valve (V1 in Figure 2), pressure signals are processed with a low-pass filter.

The flow equation for the bidirectional hydraulic pump is

$$Q_1 = Q_2 = \omega_m V_d \tag{1}$$

where Q_1 and Q_2 are the flows into and out of the pump, respectively; ω_m represents the motor speed and V_d is the pump displacement. The motor speed equation is

$$\dot{\omega}_m = \tau_m(-\omega_m + K_m u) \tag{2}$$

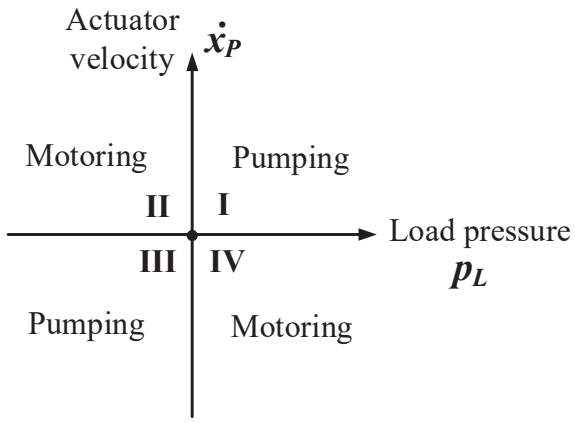

Figure 3 Four-quadrant working domain (Actuator velocity $\dot{x_p}$versus load pressure $p_L(p_L = p_a - A_b p_b/A_a)$).

In (2), K_m and τ_m are the servomotor gain and the time constant, respectively; u represents the input voltage to the servomotor. The area ratio of actuator is

$$\alpha = A_b/A_a \tag{3}$$

where A_a is piston area (cap side) and A_b is the annulus area (rod side). The load pressure is defined as

$$p_L = p_a - \alpha p_b \tag{4}$$

where p_a and p_b are the hydraulic pressures in chambers a and b, respectively. Conservation of mass can then be applied to sides a and b of the actuator, resulting in

$$Q_1 + Q_{ac} = Q_a = A_a \dot{x}_p + \frac{V_{oa} + A_a x_p}{\beta_e} \dot{p}_a \tag{5}$$

$$Q_{bc} - Q_2 = -Q_b = -A_b \dot{x}_p + \frac{V_{ob} - A_b x_p}{\beta_e} \dot{p}_b \tag{6}$$

where Q_{ac} and Q_{bc} are the compensation flows coming from the charge pump through the directional and flow-control valves to the actuator sides, a and b, respectively; Q_a and Q_b are the flows into and out of the actuator, respectively; x_p and $\dot{x}_p$ are the displacement and the velocity of the piston, respectively; β_e is the effective bulk modulus; V_{oa} and V_{ob} represent the inner pipe and cylinder chamber volumes at the two sides of actuator. Assuming

that the piston is moving within the vicinity of actuator midstroke, the following approximation can be made (Niksefat and Sepehri, 2001, Niksefat and Sepehri, 2002)

$$\frac{V_{oa} + A_a x_p}{\beta_e} \approx \frac{V_{ob} - A_b x_p}{\beta_e} \approx \frac{V_{oa} + V_{ob}}{2\beta_e} = C \tag{7}$$

where C is the hydraulic compliance. The equation describing the dynamics of the piston is

$$m_{rod}\ddot{x}_p = A_a p_L - f\dot{x}_p - F_L \tag{8}$$

In (8), $\ddot{x}_p$ is actuator acceleration; m_{rod} represents the piston rod mass; f is the viscous damping coefficient and F_L is the load force, which can be resistive or assistive, depending on the cylinder motion.

When the actuator is extending (Quadrants I and II in Figure 3), the charge pump alternately supplies an oil flow to the cap and rod sides of the actuator through V2. The following equation can then be written (Daher and Ivantysynova, 2014)

$$Q_b = \alpha Q_a \tag{9}$$

Combining (3), (4), (5), (6), (7) and (9), the following equation can be obtained

$$(1 + \alpha^2)Q_a = (1 + \alpha^2)A_a\dot{x}_p + C\dot{p}_L \tag{10}$$

In Quadrant I, $p_L > 0$ and $Q_{ac} = 0$. Performing a Laplace transformation on (1), (2), (5), (8) and (10), the following plant transfer function, $P_1(s)$, which relates the piston velocity $sX_p(s)$ to the control signal $U(s)$, can be obtained:

$$P_1(s) = \frac{sX_p(s)}{U(s)} = \frac{(1 + \alpha^2)A_a V_d \tau_m K_m}{(s + \tau_m)[m_{rod}Cs^2 + Cfs + (1 + \alpha^2)A_a^2]} \tag{11}$$

In Quadrant II, $p_L < 0$ and $Q_{bc} = 0$. From (1), (2), (6), (8), (9) and (10), we obtain the following plant transfer function $P_2(s)$:

$$P_2(s) = \frac{sX_p(s)}{U(s)} = \frac{(1 + \alpha^2)A_a V_d \tau_m K_m/\alpha}{(s + \tau_m)[m_{rod}Cs^2 + Cfs + (1 + \alpha^2)A_a^2]} \tag{12}$$

When the actuator is retracting (Quadrants III and IV in Figure 3), the oil flows from either sides of the actuator to the tank through valves V1, V2 and the relief valve.

In Quadrant IV, $p_L > 0$ and $Q_{ac} = 0$. The flow through the orifice at V2 is

$$Q_{bc} = -C_V\sqrt{(p_b - p_0)/sg} \tag{13}$$

where C_V is valve flow coefficient; Sg is the specific gravity of the fluid and p_0 is the cracking pressure of the relief valve. Linearizing (13), Q_{bc} can be expressed as

$$Q_{bc} = -K_b p_b \tag{14}$$

where K_b is the pressure sensitivity gain at the flow-control valve, given by

$$K_b = \frac{C_V}{2\sqrt{sg(p_{b0} - p_0)}} \tag{15}$$

In (15), p_{bo} is the value of p_b at operating points. Using (1) to (8) and (14), the plant transfer function $P_3(s)$ can be expressed as

$$P_3(s) = \frac{sX_p(s)}{U(s)} = \frac{(1+\alpha)A_a C V_d \tau_m K_m s + A_a K_b V_d \tau_m K_m}{(s+\tau_m)\{m_{rod}C^2 s^3 + (m_{rod}CK_b + fC^2)s^2 + [fCK_b + (1+\alpha^2)A_a^2 C]s + K_b A_a^2\}} \tag{16}$$

In Quadrant III, $p_L < 0$ and $Q_{bc} = 0$, and Q_{ac} can also be linearized as

$$Q_{ac} = -K_a p_a \tag{17}$$

where the pressure sensitivity gain at the flow-control valve, K_a, is given by

$$K_a = \frac{C_V}{2\sqrt{sg(p_{a0} - p_0)}} \tag{18}$$

In (18), p_{ao} is the value of p_a at operating points. Using (1) to (8) and (17), the plant transfer function, $P_4(s)$, can be obtained as

$$P_4(s) = \frac{sX_p(s)}{U(s)} = \frac{(1+\alpha)A_a C V_d \tau_m K_m s + \alpha A_a K_a V_d \tau_m K_m}{(s+\tau_m)\{m_{rod}C^2 s^3 + (m_{rod}CK_a + fC^2)s^2 + [fCK_a + (1+\alpha^2)A_a^2 C]s + \alpha^2 K_a A_a^2\}} \tag{19}$$

With reference to transfer functions (11), (12), (16) and (19), the hydraulic operation mode model switches due to changes in the direction of load pressure, p_L, or actuator velocity, $\dot{x}_p$. In order to include all four operation modes, the system model can be defined as $P(s) \in \{P_1(s), P_2(s), P_3(s), P_4(s)\}$.

Experimental Setup

The experimental setup is an instrumented John Deere JD-48 backhoe, as shown in Figure 4. Different load masses are used to generate a wide range of load forces (resistive or assistive) during the actuator movement. The actuator position is measured by an incremental encoder, and its velocity is calculated from data with 100-point regression.

The linkage schematic is shown in Figure 4(b). The load force, F_L, was generated by the pendular motion of the backhoe arm, described by the following equation.

$$F_L = m_L g l_2 \sin\theta / (l_1 \cos\theta) \tag{20}$$

In (20), θ is rotational angle; l_1 and l_2 are lengths of effort arm and load arm, respectively; g is gravitational acceleration; x_p and θ are geometrically related.

Values of V_d, A_a, α and Sg were obtained from the manufacturer. Values of τ_m, K_m, f, C_V, K_a and K_b were obtained from experiments. The variation in C reflects the changes in β_e and the fluid volume at each side of the actuator. An uncertainty in m_{rod} is also considered. In order to create a wide range of forces F_L, the load mass m_L is allowed to change from zero to a maximum value. The parameters of the system and the selected range of operational values are shown in Table 1. Note that system responses are significantly affected by motor dynamics, because the sensitivities of P to the variations in K_m and τ_m are high. Other parameters have less dominant effect on the magnitude of P.

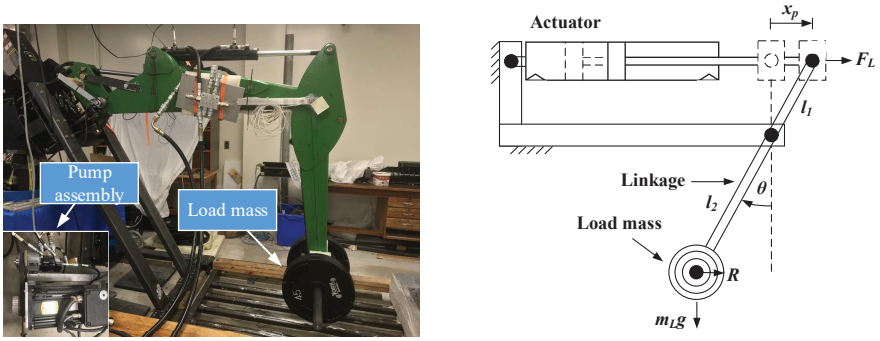

(a) (b)

Figure 4 Experimental setup. (a) Photograph of the experimental test bench. (b) Schematic of linkage attached to actuator.

Table 1 Parameters of the electro-hydrostatic actuator system

Parameter	Symbol	Value	
		Nominal	Range
Displacement of bidirectional pump (m^3/rev)	V_d	8×10^{-6}	–
Time constant of the servo motor (1/s)	τ_m	3	$2.3 - 4.0$
Servomotor gain (rev/(s·V))	K_m	5.8	$5.6 - 6.0$
Piston area (m^2)	A_a	3167×10^{-6}	–
Area ratio of actuator	α	0.75	–
Effective bulk modulus (Pa)	β_e	689×10^6	$356 \times 10^6 - 1030 \times 10^6$
Hydraulic compliance (m^3/Pa)	C	3.46×10^{-12}	$2.20 \times 10^{-12} - 7.03 \times 10^{-12}$
Piston rod mass (kg)	m_{rod}	10	$9 - 11$
Viscous damping coefficient(N·s/m)	f	900	$600 - 1200$
Valve flow coefficient($m^3/(\sqrt{}$Pa·s))	C_V	1.6×10^{-7}	–
Specific gravity of fluid	Sg	0.86	–
Pressure sensitivity gains of the orifice valve	K_a, K_b	–	$1.88 \times 10^{-10} - 37.60 \times 10^{-10}$
Load mass (kg)	m_L	–	0–163
Length of backhoe arm (m)	l	1.5	–
Length of effort arm (m)	l_1	0.3	–
Length of load arm (m)	l_2	1.2	–

Controller Design

The two degree of freedom (DOF) feedback system structure is shown in Figure 5 (Yaniv 1999, Houpis and Rasmussen, 1999). The single QFT velocity controller G is synthesized by including the plants of all four quadrants (P_1, P_2, P_3 and P_4) into a single plant P. The procedure is implemented as detailed below.

Plant Templates

QFT employs templates to capture uncertainties. Templates are frequency responses of plant P presented on the Nichols chart, considering the parametric uncertainties shown in Table 1. Figure 6 shows templates of the uncertain

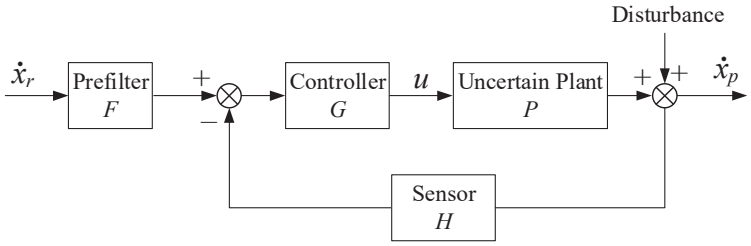

Figure 5 2-DOF feedback system structure.

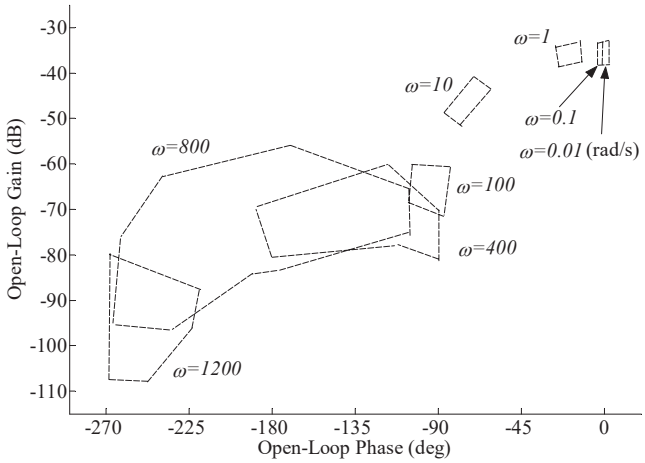

Figure 6 Plant templates at selected frequencies on the Nichols chart.

plant *P* at selected frequencies. A larger template indicates a wider range of uncertainties including modelling errors.

Tracking, Stability and Disturbance Rejection Specifications

(1) Tracking specification requires the definition of vector $\boldsymbol{\beta} = [\tau_m, K_m, C, m_{rod}, f, K_a, K_b]^T$ to express the uncertain parameters arising from changes in the system dynamics or modelling error. Therefore, the uncertain plant *P*(s) can be represented as $P(s, \boldsymbol{\beta})$. With reference to Figure 5, the closed-loop transfer function $T(s, \boldsymbol{\beta})$ is

$$T(s, \boldsymbol{\beta}) = F(s)\frac{G(s)P(s, \boldsymbol{\beta})}{1 + G(s)P(s, \boldsymbol{\beta})H(s)} \tag{21}$$

In (21), $G(s)$ and $F(s)$ are the QFT controller and prefilter, respectively. H(s) is a low-pass filter with a settling time of 0.1 s. It is employed in the design to take into account the delayed velocity measurement, caused by the regression method. $T(s, \boldsymbol{\beta})$ should satisfy the following inequality:

$$|T_L(s)| \leq |T(s, \boldsymbol{\beta})| \leq |T_U(s)| \tag{22}$$

In (22), the upper bound $T_U(s)$ has a maximum overshoot of 2% and a 2% settling time of 0.7 s; the lower bound $T_L(s)$ has no overshoot and a 2% settling time of 2.8 s. Their transfer functions are given by (23) and (24), respectively.

$$T_U(s) = \frac{(1/2.3s+1)(1/40s+1)}{(1/3s+1)(1/4s+1)(1/8s+1)} \tag{23}$$

$$T_L(s) = \frac{1}{(1/2s+1)(1/3s+1)(1/4s+1)(1/200s+1)^2} \tag{24}$$

(2) Stability specification requires the following inequality to be satisfied (Yaniv, 1999):

$$\left| \frac{G(s)P(s, \boldsymbol{\beta})H(s)}{1 + G(s)P(s, \boldsymbol{\beta})H(s)} \right| \leq 1.6(4.1 \text{ dB}) \quad \forall \boldsymbol{\omega} \in [0 \ \infty) \tag{25}$$

In (25), a gain margin of 4.22 dB and a phase margin of 36.42° are guaranteed (Yaniv, 1999).

(3) Sensitivity specification rejects disturbance. The following relation needs to be satisfied:

$$\left| \frac{1}{1 + G(s)P(s, \boldsymbol{\beta})H(s)} \right| \leq 1.8(5.1 \text{ dB}) \quad \forall \boldsymbol{\omega} \in [0 \ \infty) \tag{26}$$

The sensitivity constraint value 1.8 (5.1 dB) is determined experimentally to avoid unexpected behaviour due to the disturbance in the system, such as transitions between working quadrants or variation of the load. For higher loads, the sensitivity specification needs to change in order to maintain the robustness. This results in an increased controller complexity to prevent degraded tracking performance.

Loop Shaping and Prefilter Design

A nominal plant $P(j\omega, \boldsymbol{\beta}_0)$ is selected to move plant templates at each frequency on Nichols chart. QFT bounds are then formed when the prescribed

closed-loop specifications are satisfied (i.e., at least one specification is just satisfied and the others are over-satisfied) for the entire template. Therefore, these bounds describe the acceptable region of the nominal loop transmission $L(j\omega, \boldsymbol{\beta}_0) = G(j\omega)P(j\omega, \boldsymbol{\beta}_0)$ at corresponding frequencies, where these closed-loop specifications are satisfied despite parametric uncertainties (Yaniv, 1999; Houpis and Rasmussen, 1999). At each frequency on the Nichols chart, an open bound is satisfied if $L(j\omega, \boldsymbol{\beta}_0)$ is above or laid on it; the closed bound is satisfied if $L(j\omega, \boldsymbol{\beta}_0)$ is outside it. The bounds can be calculated using the QFT Toolbox (Borghesani et al., 2015; Ren et al., 2020). The QFT controller is then designed by shifting $L(j\omega, \boldsymbol{\beta}_0)$ until it satisfies all the bounds. The QFT bounds $B(\omega)$ and various loop transmissions $L(j\omega, \boldsymbol{\beta}_0)$, corresponding to various controllers, are shown in Figure 7. Figure 7(a) shows the $L(j\omega, \boldsymbol{\beta}_0)$ given a proportional controller having a gain 1. None of the open bounds are satisfied. In order to design a controller with a small open-loop gain and a simple structure, an integrator (with DC gain 1) is

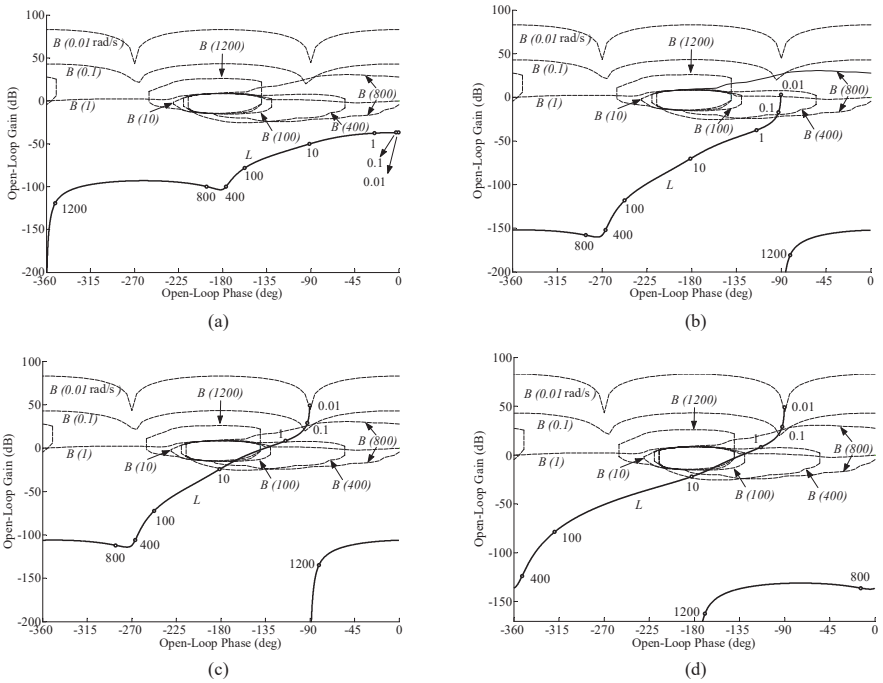

Figure 7 QFT bounds B(ω) and loop transmission $L(j\omega, \boldsymbol{\beta}_0)$ (a) $G(s) = 1$; (b) $G(s) = 1/s$; (c) $G(s) = 200/s$; (d) $G(s) = 200(1/8s + 1)/[s(1/20s + 1)^2]$.

applied. The plot of $L(j\omega, \beta_0)$, given the integral controller, is shown in Figure 7(b). Next, the integral controller gain is increased to 200 for $L(j\omega, \beta_0)$ to satisfy the open bounds. The results are shown in Figure 7(c). As is seen, open bounds are satisfied at all selected frequencies. Adding a zero to the controller further prevents the closed bounds to be violated. Finally, two poles are added to decrease the controller bandwidth. The resulting $L(j\omega, \beta_0)$ is shown in Figure 7(d). The resulting controller is given in (27). Note that the shape and size of templates can affect QFT bounds and the design of the controller.

$$G(s) = \frac{200(1/8s + 1)}{s(1/20s + 1)^2} \tag{27}$$

Note that the loop shaping described above ensures that (25), (26) are satisfied; however, (22) is only partially satisfied, as shown in (28)

$$20\log_{10}^{|T(j\omega,\boldsymbol{\beta})|_{\max}} - 20\log_{10}^{|T(j\omega,\boldsymbol{\beta})|_{\min}} \leq 20\log_{10}^{|T_U(j\omega)|} - 20\log_{10}^{|T_L(j\omega)|} \tag{28}$$

A prefilter has to be synthesized to completely satisfy (22) (Yaniv, 1999; Houpis and Rasmussen, 1999). The closed-loop responses are shown in Figure 8. With reference to Figure 8(a), in the absence of the prefilter (i.e., $F(s) = 1$), the frequency responses are above tracking bounds at some frequencies. In order to reduce the magnitudes, two poles are added. The results are shown in Figure 8(b). Finally, a complex zero is also added to shift the closed-loop frequency responses within the tracking bounds, as shown in Figure 8(c). The transfer function of the designed prefilter is given by (29).

$$F(s) = \frac{1/16s^2 + 1.6/4s + 1}{(1/2s + 1)(1/3s + 1)} \tag{29}$$

Simulation Studies

The effectiveness of the designed QFT controller, described by $G(s)$ and $F(s)$, is tested in simulations first. The ± 70 mm/s actuator step input test was conducted with a load mass of $m_L = 163$ kg attached to the linkage for system shown in Figure 4, and with nominal values of parameters given in Table 1. The normalized response is shown in Figure 9. It is seen that the step velocity response is within tracking bounds. In addition, the position response is smooth even though the actuator velocity exhibits a slight oscillation when

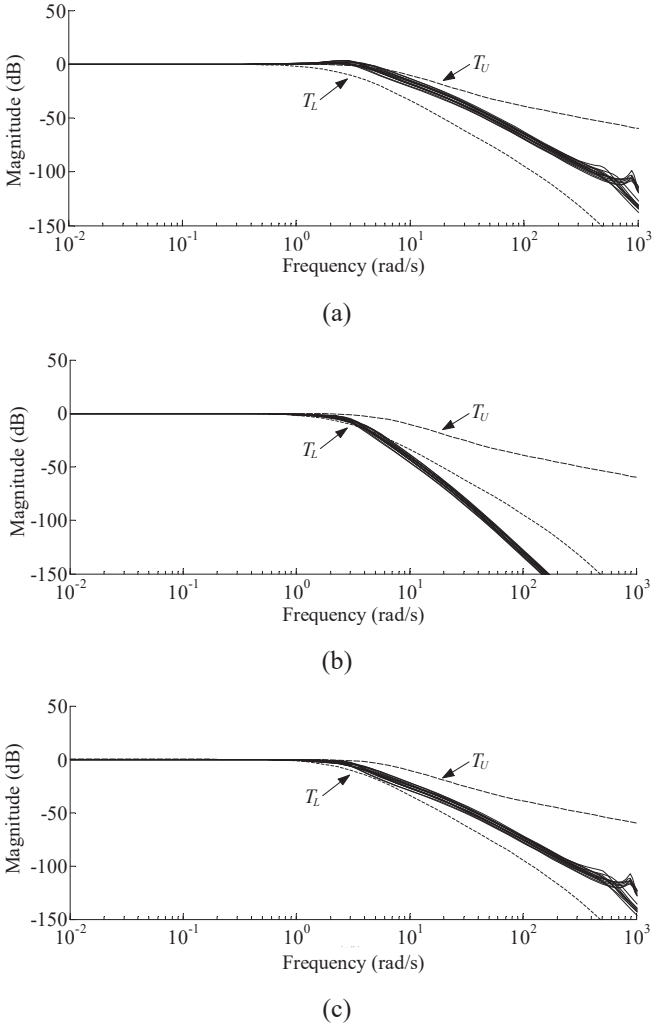

Figure 8 Closed-loop frequency responses (a) $F(s) = 1$; (b) $F(s) = 1/[(1/2s+1)(1/3s+1)]$; (c) $F(s) = (1/16s^2 + 1.6/4s + 1)/[(1/2s + 1)(1/3s + 1)]$.

the directional valve switches position. The quadrants are detected from the sign of p_L and velocity (described in Figure 3). Next, parametric uncertainties as in Table 1 were considered. Figure 10 shows the normalized velocity responses to variable actuator step inputs ranging from ± 20 to ± 70 mm/s and for the system carrying a load mass ranging from 0 kg to 163 kg. As can be

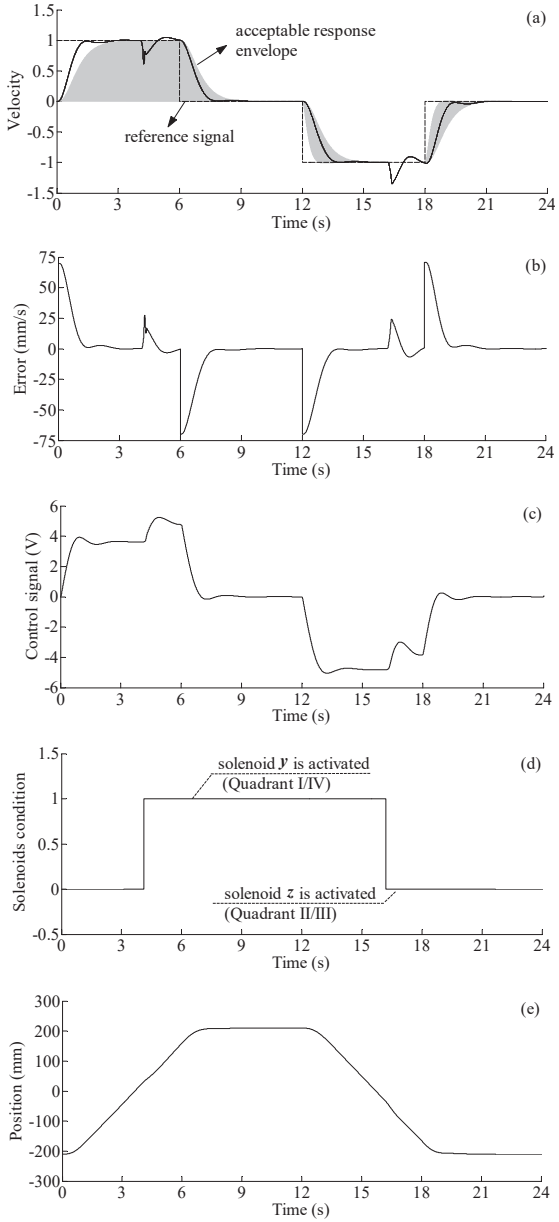

Figure 9 Simulation response to ± 70 mm/s step inputs with a load mass of 163 kg ($m_L =$ 163 kg) attached to the linkage: (a) velocity (normalized); (b) velocity error; (c) control signal; (d) solenoids' conditions of valve V1 in Figure 2; (e) actuator position.

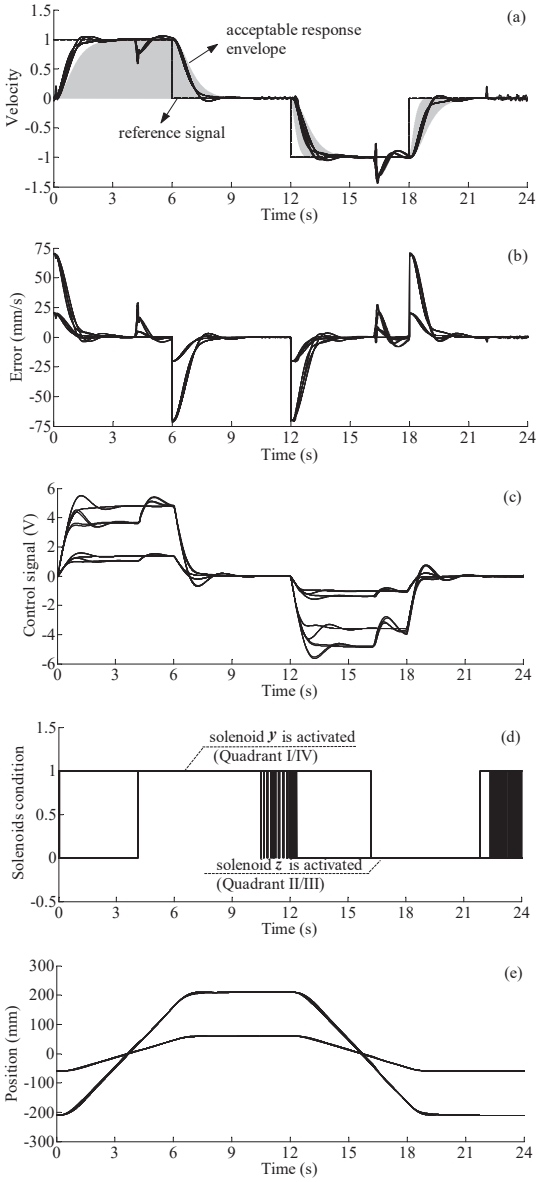

Figure 10 Simulation responses to variable step inputs ranging from ± 20 to ± 70 mm/s with a load mass ranging from 0 kg to 163 kg attached to the linkage and including parametric uncertainties in Table 1: (a) velocity (normalized); (b) velocity error; (c) control signal; (d) solenoids' conditions of valve V1 in Figure 2; (e) actuator position.

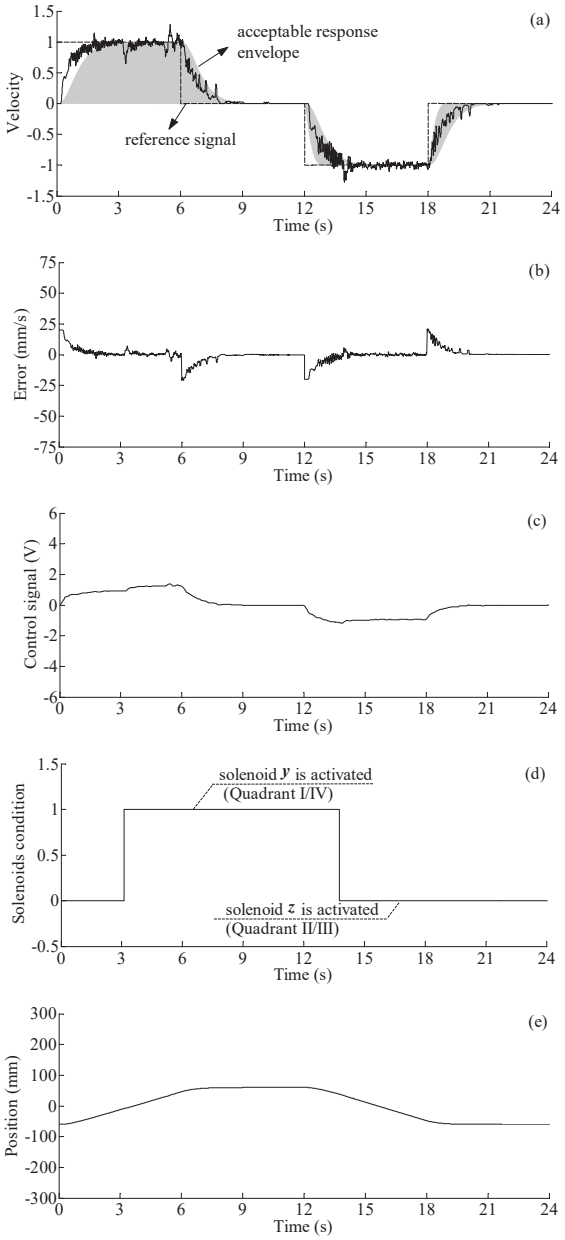

Figure 11 Experimental response to ±20 mm/s step inputs for actuator moving a 0 kg load mass: (a) velocity (normalized); (b) velocity error; (c) control signal; (d) solenoids' conditions of valve V1 in Figure 2; (e) actuator position.

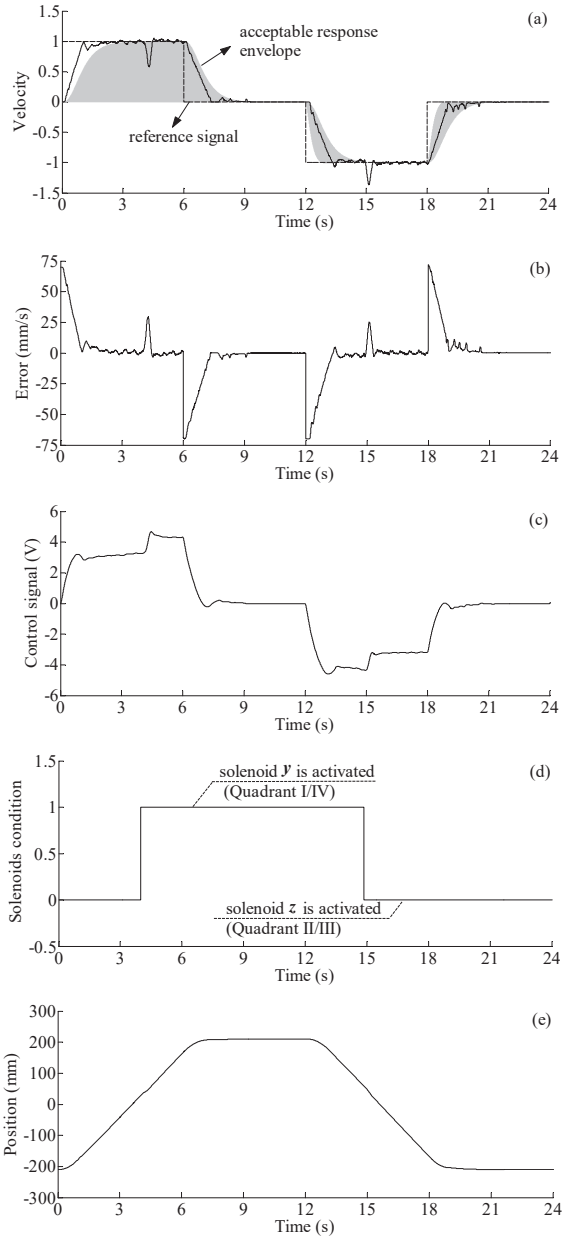

Figure 12 Experimental response to ± 70 mm/s step inputs for actuator moving a 0 kg load mass: (a) velocity (normalized); (b) velocity error; (c) control signal; (d) solenoids' conditions of valve V1 in Figure 2; (e) actuator position.

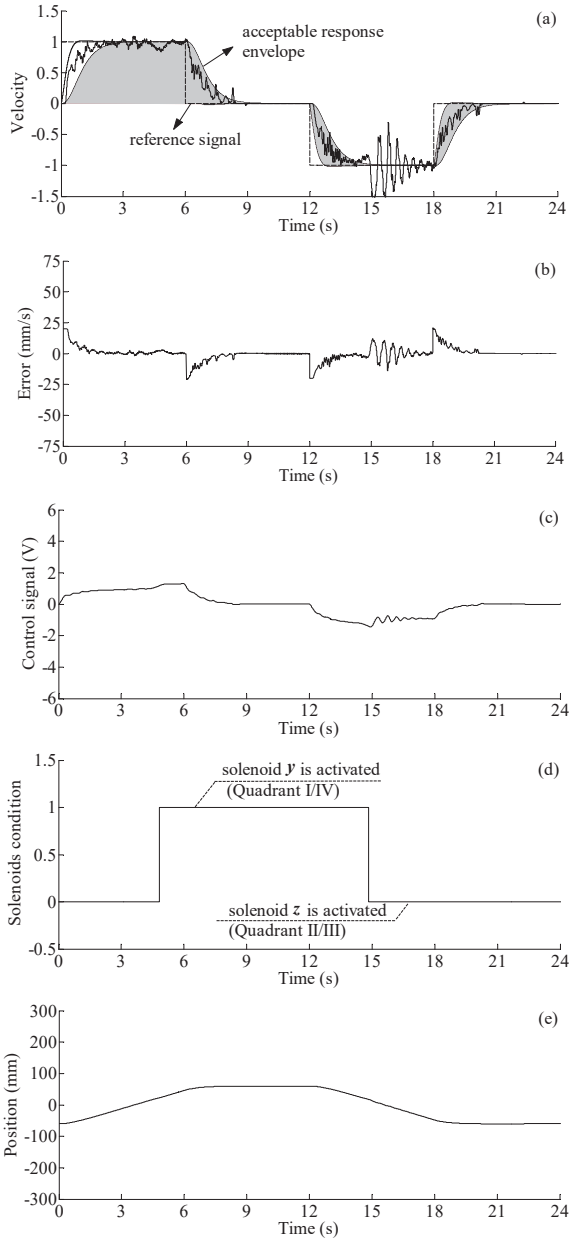

Figure 13 Experimental response to ±20 mm/s step inputs for actuator moving a 163 kg load mass: (a) velocity (normalized); (b) velocity error; (c) control signal; (d) solenoids' conditions of valve V1 in Figure 2; (e) actuator position.

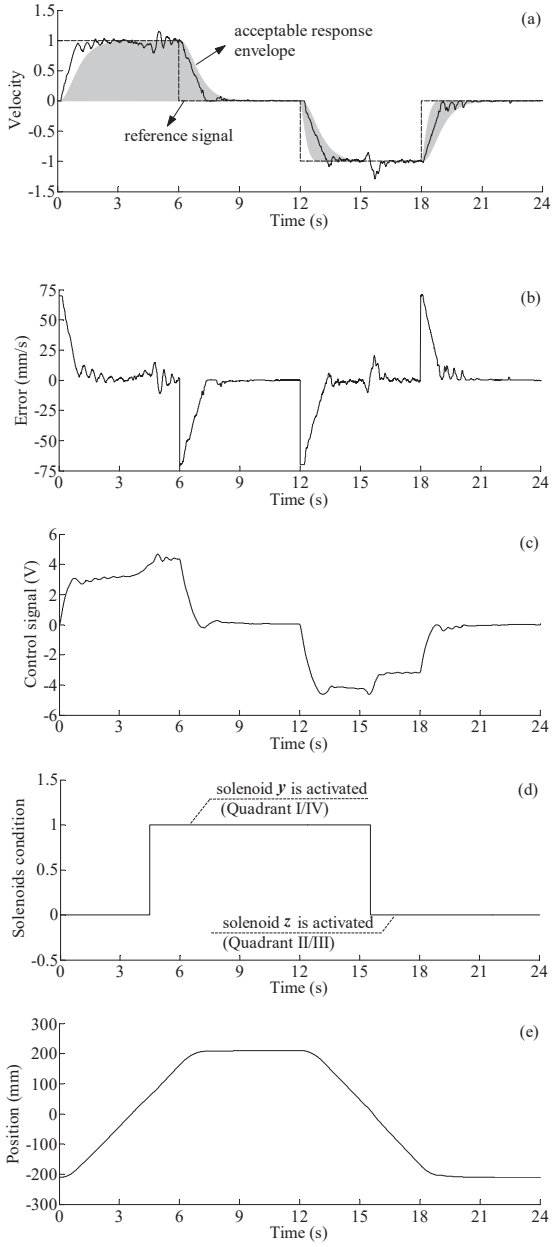

Figure 14 Experimental response to ± 70 mm/s step inputs for actuator moving a 163 kg load mass: (a) velocity (normalized); (b) velocity error; (c) control signal; (d) solenoids' conditions of valve V1 in Figure 2; (e) actuator position.

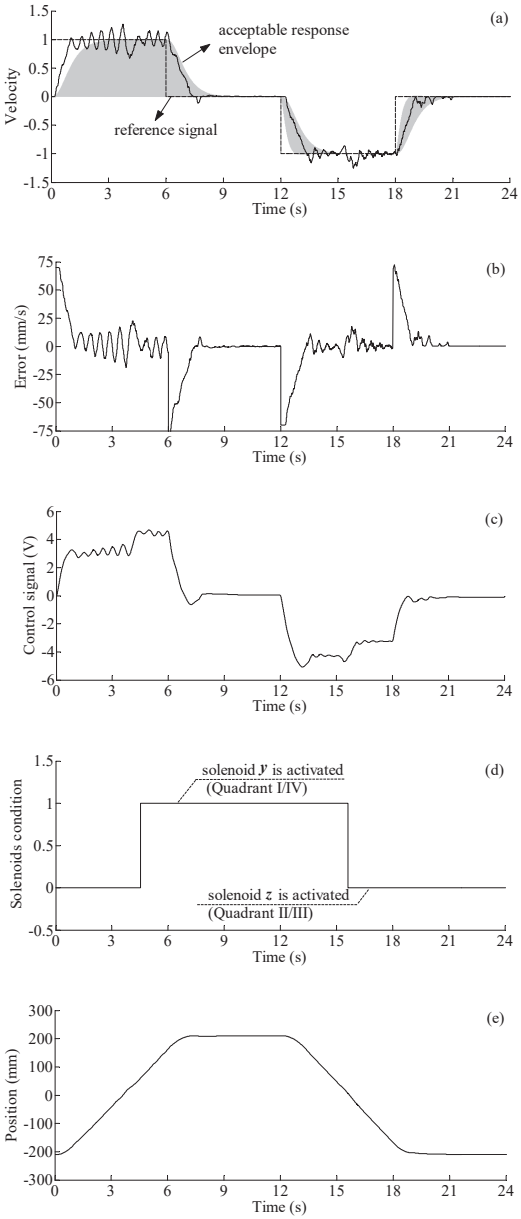

Figure 15 Experimental response to ± 70 mm/s step inputs for actuator moving a 326 kg load mass: (a) velocity (normalized); (b) velocity error; (c) control signal; (d) solenoids' conditions of valve V1 in Figure 2; (e) actuator position.

seen, good performances were obtained and the robustness of the controller is verified.

Experimental Validations

The controller was tested for $\pm$20mm/s and $\pm$70mm/s actuator velocity step inputs with a load mass of 0 kg and 163 kg attached to the linkage shown in Figure 4. The corresponding normalized velocity responses are shown in Figures 11 to 14. The velocity responses are within upper and lower bounds. However, when the solenoids' status changes, slight velocity oscillation appears. Higher load masses aggravate this phenomenon. Such undesired behaviour did not show visible effect on position responses. Figure 15 shows the results of the system carrying load of 326 kg. The velocity response exhibited slightly increased oscillations; yet, the position response shows acceptable behaviour. Note the controller was designed for load ranging from 0 kg to 163 kg. Increasing the uncertainty range at the QFT controller design stage can improve the response but may lead to a new controller structure.

Conclusions

A QFT velocity controller was designed, for the first time, for a newly developed single-rod pump-controlled actuator that operates in four quadrants. The controller guarantees tracking, stability and sensitivity specifications for a wide range of parametric uncertainties including $\pm$4% and $\pm$34% changes in servomotor gain and time constant, respectively, $\pm$50% uncertainty in effective bulk modulus of hydraulic fluid, and $\pm$34% variations in viscous damping.

Various step velocity responses were carried out using various loads. The experimental results showed that the actuator responses were maintained within tracking bounds for loads as high as 163 kg. When the directional valve switched position, the actuator velocity oscillated slightly. This oscillation was more notable with increased load mass. Nevertheless, position smoothness was not affected. Additionally, the system still performed well for loads higher than 163 kg. The results of this paper could be used for many applications where velocity control of a single-rod hydraulic actuator is required. One relevant application is teleoperation of excavators feller bunchers, where the operator controls the speed (direction and magnitude)

of the implement via a joystick (commonly known as resolved-mode control) to perform a task.

References

Ahn, K. K. and Dinh, Q. T., 2009. Self-tuning of quantitative feedback theory for force control of an electro-hydraulic test machine. *Control Engineering Practice*, 17(11), 1291–1306. DOI: 10.1016/j.conengprac.2009.06.004.

Ahn, K. K., Nam, D. N. C., and Jin, M., 2014. Adaptive backstepping control of an electrohydraulic actuator. *IEEE/ASME Transactions on Mechatronics*, 19(3), 987–995. DOI: 10.1109/TMECH.2013.2265312.

Borghesani, C., Chait, Y., and Yaniv, O., 2015. QFT Frequency Domain Control Design Toolbox [software]. Control in Biomedical Systems Research Laboratory.

Costa, G. K. and Sepehri, N., 2019. Four-quadrant analysis and system design for single-rod hydrostatic actuators. *Journal of Dynamic Systems, Measurement, and Control*, 141(2), 021011/1–021011/15. DOI: 10.1115/1.4041382.

Çalışkan, H., Balkan, T., and Platin, B. E., 2015. A complete analysis and a novel solution for instability in pump controlled asymmetric actuators. *Journal of Dynamic Systems, Measurement, and Control*, 137(9), 091008/1–091008/14. DOI: 10.1115/1.4030544.

Daher, N. and Ivantysynova, M., 2013. System synthesis and controller design of a novel pump controlled steer-by-wire system employing modern control techniques. *In: Proceedings of the ASME/BATH 2013 symposium on fluid power and motion control*. Sarasota, USA.

Daher, N. and Ivantysynova, M., 2014. An indirect adaptive velocity controller for a novel steer-by-wire system. *Journal of Dynamic Systems, Measurement, and Control*, 136(5), 051012/1–051012/9. DOI: 10.1115/1.4027172.

Daher, N. and Ivantysynova, M., 2015. Yaw stability control of articulated frame off-highway vehicles via displacement controlled steer-by-wire. *Control Engineering Practice*, 45, 46–53. DOI: 10.1016/j.conengprac.2015.08.011.

Daher, N., Wang, C., and Ivantysynova, M., 2013. Novel energy-saving steer-by-wire system for articulated steering vehicles: a compact wheel loader case study. *In: 13th Scandinavian international conference on fluid power*. Linköping, Sweden.

Hewett, A. J., 1994. Hydraulic circuit flow control. U.S. Patent 5329767.

Houpis, C. H. and Rasmussen, S. J., 1999. *Quantitative Feedback Theory: Fundamentals and Applications*. Marcel Dekker, New York, USA.

Niksefat, N. and Sepehri, N., 2001. Designing robust force control of hydraulic actuators despite system and environmental uncertainties," *IEEE Control Systems*, 21(2), 66–77. DOI: 10.1109/37.918266.

Niksefat, N. and Sepehri, N., 2002. A QFT fault-tolerant control for electrohydraulic positioning systems," *IEEE Transactions on Control Systems Technology*, 10(4), 626–632. DOI: 10.1109/TCST.2002.1014682.

Quan, Z., Quan, L., and Zhang, J., 2014. Review of energy efficient direct pump controlled cylinder electro-hydraulic technology. *Renewable and Sustainable Energy Reviews*, 35, 336–346. DOI: 10.1016/j.rser.2014.04.036.

Rahmfeld, R. and Ivantysynova M., 2000. Development and control of energy saving hydraulic servo drives. *In: Proceedings of the 1st FPNI-PhD Symposium*. Hamburg, Germany.

Ren, G., *et al*., 2016. Position control of an electrohydrostatic actuator with tolerance to internal leakage. *IEEE Transactions on Control Systems Technology*, 24(6), 2224–2232. DOI: 10.1109/TCST.2016.2517568.

Ren, G., Costa, G. K., and Sepehri, N., 2020. Position control of an electrohydrostatic asymmetric actuator operating in all quadrants. *Mechatronics*. 67, 102344. DOI: 10.1016/j.mechatronics.2020.102344.

Ren, G., Song, J., and Sepehri, N., 2017. Fault-tolerant actuating pressure controller design for an electro-hydrostatic actuator experiencing a leaky piston seal. *Journal of Dynamic Systems, Measurement, and Control*, 139(6), 061004/1-061004/8. DOI: 10.1115/1.4035348.

Ren, G., Song, J., and Sepehri, N., 2018. Design of a low-bandwidth position controller based on system identification for an electro-hydrostatic actuator. *Proceedings of the Institution of Mechanical Engineers, Part I: Journal of Systems and Control Engineering*, 232(2), 149–160.

Truong, D. Q. and Ahn, K. K., 2009. Self-tuning quantitative feedback theory for parallel force/position control of electro-hydrostatic actuators. *Proceedings of the Institution of Mechanical Engineers, Part I: Journal of Systems and Control Engineering*, 223(4), 537–556. DOI: 10.1243/09596518JSCE700.

Wang, L., Book, W. J., and Huggins, J. D., 2012. A hydraulic circuit for single rod cylinders. *Journal of Dynamic Systems, Measurement, and Control*, 134(1), 011019/1–011019/11. DOI: 10.1115/1.4004777.

Wei, S. G., et al., 2009. Self-tuning dead-zone compensation fuzzy logic controller for a switched-reluctance-motor direct-drive hydraulic

press. *Proceedings of the Institution of Mechanical Engineers, Part I: Journal of Systems and Control Engineering*, 223(5), 647–656. DOI: 10.1243/09596518JSCE720.

Williamson, C., Lee, S., and Ivantysynova, M., 2009. Active vibration damping for an off-road vehicle with displacement controlled actuators. *International Journal of Fluid Power*, 10(3), 5–16. DOI: 10.1080/14399776.2009.10780984.

Yaniv, O., 1999. *Quantitative Feedback Design of Linear and Nonlinear Control Systems*. Kluwer, Norwell, USA.

Zhang, J. and Chen, S., 2014. Modelling and study of active vibration control for off-road vehicle. *Vehicle System Dynamics*, 52(5), 581–607. DOI: 10.1080/00423114.2013.848988.

Biographies

Guangan Ren received his BSc and MSc degrees in Mechanical Engineering from Shenyang University of Technology and Northeastern University, China, in 2009 and 2011, respectively. He received his PhD in 2020 from the University of Manitoba, Canada. His research interests include robust control, system identification, energy efficient fluid power systems, and the automation of electro-hydrostatically actuated machines.

Gustavo Koury Costa is currently a Fluid Power and Fluid Mechanics Professor at the Mechanical Engineering Department at the Federal Institute of Education, Science and Technology in Recife-PE, Brazil. He received his MSc and DSc degrees from the Federal University of Pernambuco, Brazil and held Post-Doctorates in The University of Manitoba, Canada.

Nariman Sepehri is a professor with the Department of Mechanical Engineering, at the University of Manitoba, Canada. He received MSc and PhD degrees from the University of British Columbia, Canada. His research and development activities are primarily centred in all fluid power-related aspects of systems, manipulation, diagnosis, and control.